Published in final edited form as:
Magn Reson Imaging. 2013 February ; 31(2): 227–234. doi:10.1016/j.mri.2012.06.016.

Detecting peritoneal dissemination of ovarian cancer in mice by DWIBS

Hye Jeong Lee[a,b,*], **Jeffrey J. Luci**[c], **Mohammed N. Tantawy**[a,b], **Haakil Lee**[d], **Ki Taek Nam**[e], **Todd E. Peterson**[a,b,f], and **Ronald R. Price**[a,b]

[a]Department of Radiology and Radiological Sciences, Vanderbilt University Medical Center, Nashville, TN 37232, USA

[b]Institute of Imaging Science, Vanderbilt University Medical Center, Nashville, TN 37232, USA

[c]Imaging Research Center and Section of Neurobiology, University of Texas at Austin, Austin, TX 78712, USA

[d]Department of Chemical Engineering, University of Keimyung, 1095 Dalgubeol-daero Daegu, South Korea 704-701

[e]Department of Surgery, Vanderbilt University Medical Center, Nashville, TN 37232, USA

[f]Program in Chemical and Physical Biology, Vanderbilt University Medical Center, Nashville, TN 37232, USA

Abstract

Diffusion-weighted whole-body imaging with background body signal suppression (DWIBS) is a relatively new diffusion-based pulse sequence that produces positron emission tomography (PET) with 2-[fluorine-18]-fluoro-2-deoxy-D-glucose (^{18}F-FDG)-like images. We tested the feasibility of DWIBS in detecting peritoneal ovarian cancer in a syngeneic mouse model. Female C57BL/6 mice were injected intraperitoneally with ID8 murine ovarian carcinoma cells. After 11 weeks, the abdomen was imaged by DWIBS. A respiratory gating diffusion-weighted spin-echo echo-planar imaging in abdomen was used (imaging parameters of field of view of 47×47 mm^2, matrix size of 64×64 zero-filled to 256×256 and *b*-value of 1500 s/mm^2). We also performed FDG microPET as the reference standard. For comparison of the correlating surface areas of tumor foci on both DWIBS and FDG microPET imaging, two-dimensional region-of-interest (ROI) analysis was performed, and correlation between the two modalities was determined. Mice were also subjected to macroscopic examination for tumor location and pathology after imaging. DWIBS in all mice depicted the tumors as abnormal high signal intensity. The results show that the ROI analysis of correlating lesions reveals relatively high correlation (r^2=0.7296) and significant difference (*P*=.021) between DWIBS and FDG microPET. These results demonstrate that DWIBS has the potential for detecting peritoneal dissemination of ovarian cancer. Nonetheless, due to low ratios of image signal-to-noise and motion artifacts, DWIBS can be limited for lesions near the liver.

Keywords

Ovarian cancer; Syngeneic mouse model; DWIBS; ^{18}F-FDG; microPET

* Corresponding author. Department of Radiology and Radiological Sciences, Vanderbilt University Medical Center, Nashville, TN 37232–2675, USA. Tel.: +1 615 322 3190; fax: +1 615 322 3764. hye-jeong.lee@vanderbilt.edu (H.J. Lee)..

1. Introduction

Ovarian cancer metastasis is one of the gynecological malignancies with the characteristics of widespread peritoneal tumor dissemination [1]. Such random peritoneal tumors are difficult to detect in conventional anatomical magnetic resonance imaging (MRI) or computed tomography (CT) due to poor differentiation of the tumor from the surrounding organs and small tumor size [2,3]. Accordingly, the imaging tools that can provide functional information of the tumor have been suggested to be more effective. Positron emission tomography (PET) using 2-[fluorine-18]-fluoro-2-deoxy-D-glucose (^{18}F-FDG) provides metabolic information on glucose metabolism, and PET combined with CT is currently an established multimodal imaging technique useful in clinical oncology [4,5]. PET/CT imaging is sensitive and specific in the early detection of recurrent ovarian cancer and thus has the potential to monitor response to chemotherapy [6,7]. However, PET provides false-positive results because the tracer ^{18}F-FDG can be physiologically taken up by nonpathological organs, such as the kidney, heart, liver, stomach and gut [8–10]. PET also requires long preparation and imaging times, as well as exposure to ionizing radiation for examination. PET has difficulty accurately localizing pathological tissue due to misregistered PET and CT images caused by respiratory motion artifacts [11,12].

Diffusion-weighted magnetic resonance imaging (DWI) is based on the random motion of water molecules in biological tissues. DWI provides functional information related to cellular architecture density and pathological changes. The major advantages of DWI is not calling for the administration of an exogenous contract agent and not exposing patients to ionizing radiation. These advantages especially become more important in case of patients who are required for repetitive image measurements. In 2004, a new diffusion-based pulse sequence diffusion-weighted whole-body imaging with background body signal suppression (DWIBS) was introduced to allow noninvasive screening of the whole body [13]. DWIBS is an entirely different technology from FDG microPET, but their images are visually quite similar [14–19]. Another advantage of DWIBS is that it can reduce the probability of a mismatch between anatomical and functional data sets. For these reasons, DWIBS has the potential to be a powerful and convenient method for cancer assessment.

DWIBS has shown to be useful for detecting and characterizing tumors and evaluating treatment response. However, in order to establish it in the clinic, more studies are needed to evaluate the value of DWIBS. It is particularly interesting to compare DWIBS with other established imaging modalities, such as single photon emission computed tomography (SPECT)/CT, PET/CT and conventional MRI [20,21]. In this study, we tested the feasibility of DWIBS for detecting peritoneal ovarian cancer in mice, which was compared with FDG microPET findings used as a reference modality.

2. Materials and methods

2.1. Syngeneic mouse model

All animal studies were conducted following review and approval by the Vanderbilt University Institutional Animal Care and Usage Committee. Five female C57BL/6 mice (6–8 weeks, weighting 18–20 g) were purchased from Harlan Laboratories (Indianapolis, IN, USA). Peritoneal metastasis of ovarian cancer was induced as described previously [10]. Briefly, seven million ID8 cells, which are transformed tumorigenic cells originated from C57BL/6 mice [22], were injected intraperitoneally into each mouse. All mice showed high focal uptake of FDG in microPET images at 11 weeks after tumor cell injection. The lesions were confirmed as tumors by pathological examination [10].

2.2. MicroPET, microCT and MRI

All imaging studies were performed in the Center for Small Animal Imaging at Vanderbilt University Institute of Imaging Science. MicroPET and microCT were carried out following procedures described previously [10]. Briefly, for microPET imaging, after fasting overnight, each mouse was injected intravenously with approximately 7.4 MBq of ^{18}F-FDG. Forty minutes postinjection of FDG, the mouse was imaged for 20 min in a microPET Focus 220 (Siemens, Knoxville, TN, USA). All coronal images were reconstructed using the maximum a posteriori algorithm supplied with the scanner with a beta (smoothing) value of 0.1 with 18 iterations into transaxial slices (128×128×95) with voxel sizes of 0.05×0.05×0.08 cm^3. Immediately after microPET imaging, the mouse on the animal holder was transferred directly to the microCAT II (Siemens, Knoxville, TN, USA) and imaged for approximately 10 min using a tube voltage of 80 kVp and a current of 500 μA at an exposure rate of 300 ms per projection with 180 projections taken over a 360° rotation of the gantry.

The animal was then transferred to the MRI scanner in the same bed position. MRI was performed on a Varian DirectDrive 4.7-T MRI system (Varian, Palo Alto, CA, USA) with a 38-mm Litz cage RF coil (Doty Scientific, Columbia, SC, USA). Standard T_2-weighted coronal (magnet frame of reference) multislice images of the abdomen of mice were acquired using respiratory gating and a field of view (FOV) of 47×47 mm^2, a slice thickness of 1 mm and a matrix size of 256×128, zero-filled to 256×256. The optimum inversion time to null fat in an inversion recovery (IR) sequence was found to be 225 ms and used for DWIBS imaging. The DWIBS images were acquired with the same coronal FOV used for the T_2-weighted images, but without slice selection in order to acquire a projection image. Prior publications [13,19–21] on DWIBS most commonly acquire multiple axial images that are processed to produce projection images at any desired angle. For our study, we chose to use a coronal projection for comparison to the corresponding microPET images. The sequence was an IR-prepared spin-echo echo-planar imaging (EPI) with diffusion weighting. Respiratory gating was used, and the echo time (TE) was 26.4 ms. The diffusion-sensitizing gradient parameters were δ=6 ms, Δ=16.5 ms and G_{diff}=20.04 G/cm, all corresponding to a resultant b-value of 1500 s/mm^2. DWIBS studies [13,17,20] have typically been performed at 1.5 T using TE on the order of 70 ms and b-values of 1000 s/mm^2. Studies in the prostate [23] were found to provide better sensitivity as b-values of up to 2000 s/mm^2 are used. With the increased signal at 4.7 T and shorter TE of 26.4 ms, we found the b-value of 1500 s/mm^2 to provide appropriate image quality and contrast between what we thought were tumors and the surrounding parenchymal tissue. The k-space trajectory was centric and traversed in four shots. Since a triple reference scan was used to minimize the $n/2$ ghosting in the reconstructed images, four repetitions per shot were acquired. The matrix size was 64×64 zero filled to 256×256 to allow for intrinsic co-registration with the T_2-weighted image. The acquisition time was 12 min, and all DWIBS images were provided with color-coded contrast display.

2.3. Image data analysis

For image analysis, any distinct foci with excessive ^{18}F-FDG accumulation or increased signal intensity when compared with the intensity of the background were considered to be a potential lesion. Each potential lesion was then confirmed by pathological examination. For the quantitative analysis, regions of interest (ROIs) were placed on the hyperintense pixels, which exceeded the average of adjacent background pixel value, and the scalar values were obtained. For measurement of tumor surface area from microPET images, following setting the background threshold, ROIs were manually drawn around the lesions showing the high focal uptake of FDG and computed using IDL Virtural Machine 6.0 software (Research Systems, Boulder, CO, USA). For measurement of tumor surface area from DWIBS images,

ROIs were drawn around the lesions showing abnormal hyperintense signal, and the number of tumor pixels was computed using ImageJ software (National Institutes of Health, NIH). Tumor surface area was then calculated as [(number of tumor pixels)×(area of each pixel)]. For measurement of tumor volume from T_2-weighted MR images, ROIs were drawn on each image containing tumors using ImageJ and then multiplied by slice thickness to obtain the tumor volume. If tumorlike tissue was seen in several slices, then tumor volume were added together. Tumor volume was also measured from macroscopic images of mouse sacrificed after imaging; the diameters of tumors on macroscopic images were measured, and the volumes were then calculated as $4/3\times\pi\times R^3$, where R represents the diameter of tumor/2. The measurement of ROIs on a perlesion basis was performed at least three times, and the mean values were used to evaluate correlation of the two modalities: DWIBS and FDG microPET.

2.4. Histopathological examination

After MRI, mice were sacrificed for the localization of lesions to match the image data. The localization of lesions to match the image data in each mouse was evaluated. Tumors were photographed for the gross pathology. The specimens corresponding to the images were collected and fixed in neutral buffered 10% formalin. The formalin-fixed samples were embedded in paraffin and sectioned at 5-μm thickness. One slice from each block was stained with hematoxylin and eosin (H&E). The samples were examined with a Zeiss Axiophot bright-field microscope equipped with an Axiovision digital imaging system (Carl Zeiss, Thornwood, NJ, USA).

2.5. Statistical analysis

Data were obtained from ROI analyses of comparable lesions in both images of DWIBS and FDG microPET and were presented as mean±S.D. Spearman's (rho) rank correlation coefficient was computed to test for strength of correlation between DWIBS and FDG microPET. Levels of significance were assessed with paired Student's t test for comparison between two values. A P value less than .05 was considered significant. Data were analyzed using Origin 8.1 software (OriginLab, Northampton, MA, USA).

3. Results

3.1. Imaging

Fig. 1 shows ventral view images of a representative mouse that was intraperitoneally injected with ovarian surface epithelial cancer cells ID8. Images were obtained 11 weeks after injection. The lesions showing hyperintense signals were well depicted on DWIBS image (arrows; Fig. 1A). These signals were correlated with the microPET image in comparable regions (Fig. 1D). In contrast, the lesions were not clearly depicted on the T_2-weighted MR image (Fig. 1B).

Some of the signals in the DWIBS images appeared to be motion artifacts. Strong hyperintense signals were detected in DWIBS images, but some of these hyperintense signals were poorly correlated with those in the microPET images (Figs. 3A and 3D). For example, three hyperintense signals in the upper abdomen (arrowheads in Fig. 3A) were not detected at the corresponding region in microPET image (Fig. 3D). These signals along with stripes represent motion artifacts. In contrast, the strong hyperintense signals (arrows; Fig. 3A) in the lower abdomen were clearly correlated with two comparable lesions in the microPET image (arrows; Fig. 3D). In T_2-weighted MR image, three lesions were shown in the right abdomen (arrows; Fig. 3B). Among them, the first two lesions (clockwise) were correlated with the lesion in the microPET image (left arrow; Fig. 3D).

3.2. Macroscopic features

After noninvasive imaging, all mice were euthanized for macroscopic examination. Widespread peritoneal tumor dissemination and blood ascites were shown in the peritoneal cavity of all mice. These are characteristic of peritoneal dissemination of ovarian cancer [1] and also consistent with our recent report [10]. Random tumor implants were mainly present in the regions along the peritoneum (Figs. 2A and 4A & 4B).

Fig. 2A shows the macroscopic appearance of a representative mouse in peritoneal metastasis used in Fig. 1. The regions corresponding to the lesions (arrows) in the image data had tumors (circles in the figure). The average tumor volume in the left and right circle areas was 1.57±0.05 mm^3 (n=10) and 0.45±0.02 mm^3 (n=15), respectively. Fig. 4 shows the regions containing tumors. These regions corresponded to the image data in Fig. 3. The average tumor volume in the left (Fig. 4A) and right (Fig. 4B) circle areas was 0.33±0.01 mm^3 (n=17) and 0.09±0.02 mm^3 (n=23), respectively. The volumes of the three lesions in T_2-weighted MR image (arrows; Fig. 3B) were 2.01±0.02 mm^3, 1.02±0.02 mm^3 and 0.45±0.00 mm^3 (clockwise). Among them, the second and third lesions clockwise had similar tumor volumes as those for macroscopic appearance (arrows; Fig. 4A). The average tumor volume in the regions containing tumors that corresponded to the image data from all mice was 0.54±0.03 mm^3 (n=225 tumors from five mice). The biggest tumor volume (arrow; Fig. 2A) and the smallest tumor volume detectable were 1.96±0.04 mm^3 and 0.05±0.00 mm^3, respectively.

3.3. Histopathology

We also performed histopathological experiments with lesions selected in mice after macroscopic examination. The localization of lesions was matched to both DWIBS and microPET images. Tumors in the peritoneum were confirmed by staining paraffin sections with H&E (Figs. 2B and 4C).

3.4. Correlation

For correlation of DWIBS and FDG microPET imaging, relative area assessments were performed by a ROI analysis of comparable lesions in both DWIBS and FDG microPET images. Fig. 5 shows relatively high correlation with r^2=0.7296 and a significant difference between the two modalities (P=.021).

4. Discussion

In this study, we demonstrate the potential of DWIBS for the detection of peritoneal dissemination of ovarian cancer in mice. We found that DWIBS could depict tumors in all of mice we examined. We also found a significant difference between DWIBS and FDG microPET from the ROI analysis of comparable regions. These results suggest that DWIBS imaging can be a feasible tool for detecting ovarian cancer.

In this study, we used a syngeneic mouse model. Unlike xenograft models, the syngeneic model can give a more realistic tumor environment due to similar tumor induction like in humans [1]. This model of ovarian cancer creates a very widespread and disseminated carcinomatosis [1,10]. It was seen clearly from the figures that, where the imaging techniques appeared to show one or two foci of disease, there were several tiny foci. The smallest tumor volume detectable in the regions of tumors corresponding to the image data was approximately 0.05 mm^3, which might help optimize the detection rate in human subjects. However, tumors in image data were detected as clusters instead of individuals in the syngeneic model (Figs. 1A and 3A). These tumor clusters make it difficult to evaluate the limit of detection capability of the DWIBS technique. An important feature of ^{18}F-FDG

PET is that the metabolic information is available. Comparable functional information of DWIBS is the restricted water mobility within hypercellular tumors to increase the contrast between these lesions and surrounding tissues. Recently, we reported the usefulness of ^{18}F-FDG microPET imaging in tracking the growth of intraperitoneal tumor in a syngeneic mouse model [10]. This result led us to investigate the diffusion-weighted imaging that provides the other functional information, especially DWIBS, with the same animal model. Unlike xenograft models, this syngeneic model may provide more appropriate information as a preclinical animal model.

Takahara et al. [13] developed an advanced technique DWIBS using free-breathing and short TI inversion recovery (STIR). Recently, researchers have been increasingly investigating the usefulness of DWIBS for peritoneal dissemination in gynecologic malignancy [14–19]. Fujii et al. [14] evaluated the usefulness of DWIBS according to established methods [13] for the detection of peritoneal dissemination in patients with ovarian cancer. Briefly, they used 1.5-T MR system under free breathing and STIR-EPI. Images were sliced, and coronal maximum-intensity projection image was reconstructed from axial source images. On the other hand, our study was conducted using a 4.7-T MR system with animals. IR-EPI was used, but images were not sliced. Furthermore, we used respiratory gating instead of free breathing for DWIBS technique. Respiratory gating theoretically reduces motion artifact [19,24], which is specially good for visualization of small lesions on the areas near the diaphragm that may be prevented by using free breathing [24]. A good fat suppression was also done for abdomen with IR of an inversion time of 225 ms.

Despite of our demonstration of the feasibility to use DWIBS for detecting peritoneal ovarian cancer, our study has some limitations. First, the DWIBS technique is susceptible to artifacts from several causes. Artifacts tend to worsen at longer acquisition time. The respiratory gating used in this study requires a longer scan time (12 min), which can lead to induce artifacts. The DWIBS technique is also sensitive to motion influences arising from different organs [24,25], which may lead to artifacts and signal losses in the images. Even though the respiratory gating should greatly reduce motion artifacts, the images can still have artifacts. As shown in Fig. 3A, stripes appeared on the upper abdomen of the DWIBS image. These are artifacts that arise from cardiac/respiratory motion [26]. In addition, lesions may also be missed due to signal losses arising from motion. Our data also suggest that many tumor lesions detected by macroscopic appearance may not be evident in DWIBS images. Especially, signals in the liver were not shown, suggesting that the result could be attributed to signal losses that may be induced from motions of the heart/diaphragm near the liver. As shown in Fig. 3D, microPET image showed a high focal uptake of FDG in the right abdomen, that was composed of many individual tumors according to the macroscopic appearance (circle; Fig. 4A). In contrast, some tumors at the comparable regions were not detected at the the DWIBS image (Fig. 3A). In addition to motion artifacts, this phenomenon can be also attributed to either low or distorted signals near the liver/diaphragm, which might be a pitfall [25,27] related to image plane design because liver surface and subdiaphragmatic space are common sites of peritoneal tumor seeding. Another limitation of our study was in anatomical images. Many lesions were not found on T_2-weighted MR images.

Nonetheless, some of the described limitations can be abolished in human imaging. That is, since 1.5 T [13] or 3.0 T [26] magnetic strengths in the clinic are usually used, some limitations may lead to better visualization in the clinic using this method. In addition, the DWIBS sensitivity reduced by using the respiratory gating will be even better in human imaging than what we report for the mice because the use of breath-hold technique in human studies can effectively eliminate the motion artifacts.

In conclusion, our study demonstrates that DWIBS is a potential tool for detecting peritoneal dissemination of ovarian cancer. These findings suggest that DWIBS may have potential role in monitoring therapy response and possibly for the early detection of ovarian cancer. Further research will be also required to determine the minimum detectable tumor volume and its dependence on diffusion gradient strength and magnetic field strength. The results of this research will provide insight into whether or not DWIBS is useful for cancer screening.

Acknowledgments

We appreciate excellent support from the Vanderbilt University Institute of Imaging Science. We thank Dr. Dineo Khabele for discussing the ovarian cancer mouse model. We also thank Jarrod True and Jordan Fritz at the CSAI for their assistance with microPET and microCT scan, and Jeff Clanton and Jarrod Driskill for ^{18}F-FDG production. This work was supported by NIH grants NIH R25 CA092043 and NIH P30 CA68485.

References

1. Greenaway J, Moorehead R, Shaw P, Petrik J. Epithelial-stromal interaction increases cell proliferation, survival and tumorigenicity in a mouse model of human epithelial ovarian cancer. Gynecol Oncol. 2008; 108:385–94. [PubMed: 18036641]
2. Frasci G, Contino A, Iaffaioli RV, Mastrantonio P, Conforti S, Persico G. Computerized tomography of the abdomen and pelvis with peritoneal administration of soluble contrast (IPC-CT) in detection of residual disease for patients with ovarian cancer. Gynecol Oncol. 1994; 52:154–60. [PubMed: 8314132]
3. Giunta S, Tipaldi L, Diotellevi F, Squillaci E, Cecconi L, Nardis PF, et al. CT demonstration of peritoneal metastases after intraperitoneal injection of contrast media. Clin Imaging. 1990; 14:31–4. [PubMed: 2322880]
4. Bar-Shalom R, Yefremov N, Guralnik L, Gaitini D, Frenkel A, Kuten A, et al. Clinical performance of PET/CT in evaluation of cancer: additional value for diagnostic imaging and patient management. J Nucl Med. 2003; 44:1200–9. [PubMed: 12902408]
5. von Schulthess GK, Steinert HC, Hany TF. Integrated PET/CT: current applications and future directions. Radiology. 2006; 238:405–22. [PubMed: 16436809]
6. Chung HH, Kang WJ, Kim JW, Park NH, Song YS, Chung JK, et al. Role of [18F]FDG PET/CT in the assessment of suspected recurrent ovarian cancer: correlation with clinical or histological findings. Eur J Nucl Med Mol Imaging. 2007; 34:480–6. [PubMed: 17089122]
7. Simcock B, Neesham D, Quinn M, Drummond E, Milner A, Hicks RJ. The impact of PET/CT in the management of recurrent ovarian cancer. Gynecol Oncol. 2006; 103:271–6. [PubMed: 16626793]
8. Hays MT, Segall GM. A mathematical model for the distribution of fluorodeoxyglucose in humans. J Nucl Med. 1999; 40:1358–66. [PubMed: 10450689]
9. de GM, Meeuwis AP, Kok PJ, Corstens FH, Oyen WJ. Influence of blood glucose level, age and fasting period on non-pathological FDG uptake in heart and gut. Eur J Nucl Med Mol Imaging. 2005; 32:98–101. [PubMed: 15605289]
10. Lee HJ, Tantawy MN, Nam KT, Choi I, Peterson TE, Price RR. Evaluation of an intraperitoneal ovarian cancer syngeneic mouse model using 18F-FDG microPET imaging. Int J Gynecol Cancer. 2011; 21:22–7. [PubMed: 21321526]
11. Warach S, Chien D, Li W, Ronthal M, Edelman RR. Fast magnetic resonance diffusion-weighted imaging of acute human stroke. Neurology. 1992; 42:1717–23. [PubMed: 1513459]
12. Kim T, Murakami T, Takahashi S, Hori M, Tsuda K, Nakamura H. Diffusion-weighted single-shot echoplanar MR imaging for liver disease. AJR Am J Roentgenol. 1999; 173:393–8. [PubMed: 10430143]
13. Takahara T, Imai Y, Yamashita T, Yasuda S, Nasu S, Van CM. Diffusion weighted whole body imaging with background body signal suppression (DWIBS): technical improvement using free breathing, STIR and high resolution 3D display. Radiat Med. 2004; 22:275–82. [PubMed: 15468951]

14. Fujii S, Matsusue E, Kanasaki Y, Kanamori Y, Nakanishi J, Sugihara S, et al. Detection of peritoneal dissemination in gynecological malignancy: evaluation by diffusion-weighted MR imaging. Eur Radiol. 2008; 18:18–23. [PubMed: 17701040]
15. Low RN, Sebrechts CP, Barone RM, Muller W. Diffusion-weighted MRI of peritoneal tumors: comparison with conventional MRI and surgical and histopathologic findings — a feasibility study. AJR Am J Roentgenol. 2009; 193:461–70. [PubMed: 19620444]
16. Kyriazi S, Collins DJ, Morgan VA, Giles SL, deSouza NM. Diffusion-weighted imaging of peritoneal disease for noninvasive staging of advanced ovarian cancer. Radiographics. 2010; 30:1269–85. [PubMed: 20833850]
17. Satoh Y, Ichikawa T, Motosugi U, Kimura K, Sou H, Sano K, et al. Diagnosis of peritoneal dissemination: comparison of 18F-FDG PET/CT, diffusion-weighted MRI, and contrast-enhanced MDCT. AJR Am J Roentgenol. 2011; 196:447–53. [PubMed: 21257899]
18. Kyriazi S, Kaye SB, deSouza NM. Imaging ovarian cancer and peritoneal metastases — current and emerging techniques. Nat Rev Clin Oncol. 2010; 7:381–93. [PubMed: 20386556]
19. Kwee TC, Takahara T, Ochiai R, Nievelstein RA, Luijten PR. Diffusion-weighted whole-body imaging with background body signal suppression (DWIBS): features and potential applications in oncology. Eur Radiol. 2008; 18:1937–52. [PubMed: 18446344]
20. Komori T, Narabayashi I, Matsumura K, Matsuki M, Akagi H, Ogura Y, et al. 2-[Fluorine-18]-fluoro-2-deoxy-D-glucose positron emission tomography/computed tomography versus whole-body diffusion-weighted MRI for detection of malignant lesions: initial experience. Ann Nucl Med. 2007; 21:209–15. [PubMed: 17581719]
21. Stecco A, Romano G, Negru M, Volpe D, Saponaro A, Costantino S, et al. Whole-body diffusion-weighted magnetic resonance imaging in the staging of oncological patients: comparison with positron emission tomography computed tomography (PET-CT) in a pilot study. Radiol Med. 2009; 114:1–17. [PubMed: 19082787]
22. Roby KF, Taylor CC, Sweetwood JP, Cheng Y, Pace JL, Tawfik O, et al. Development of a syngeneic mouse model for events related to ovarian cancer. Carcinogenesis. 2000; 21:585–91. [PubMed: 10753190]
23. Metens T, Miranda D, Absil J, Matos C. What is the optimal b value in diffusion-weighted MR imaging to depict prostate cancer at 3T? Eur Radiol. 2012; 22(3):703–9. Epub 2011 Oct 5. [PubMed: 21971824]
24. Kwee TC, Takahara T, Koh DM, Nievelstein RA, Luijten PR. Comparison and reproducibility of ADC measurements in breathhold, respiratory triggered, and free-breathing diffusion-weighted MR imaging of the liver. J Magn Reson Imaging. 2008; 28:1141–8. [PubMed: 18972355]
25. Le BD, Poupon C, Amadon A, Lethimonnier F. Artifacts and pitfalls in diffusion MRI. J Magn Reson Imaging. 2006; 24:478–88. [PubMed: 16897692]
26. Murtz P, Krautmacher C, Traber F, Gieseke J, Schild HH, Willinek WA. Diffusion-weighted whole-body MR imaging with background body signal suppression: a feasibility study at 3.0 Tesla. Eur Radiol. 2007; 17:3031–7. [PubMed: 17646990]
27. De Gaetano AM, Calcagni ML, Rufini V, Valenza V, Giordano A, Bonomo L. Imaging of peritoneal carcinomatosis with FDG PET-CT: diagnostic patterns, case examples and pitfalls. Abdom Imaging. 2009; 34:391–402. [PubMed: 18446399]

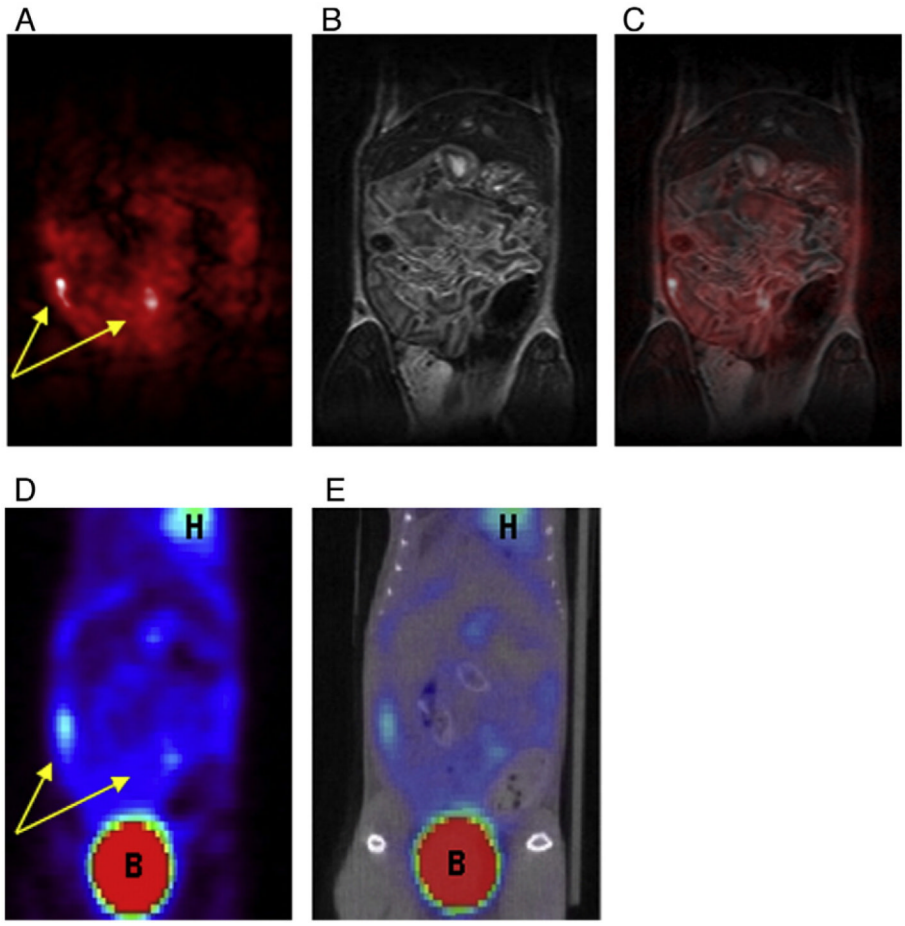

Fig. 1.

Coronal images of a mouse at 11 weeks after tumor cell injection. Color-coded DWIBS image (A) was obtained by using IR fat suppression at 4.7 T, highlighting two lesions (arrows). T_2-weighted MR image is shown in (B), and fusion image of DWIBS and T_2-weighted image is shown in (C). Two hyperintense signals (arrows) on FDG microPET image (D) were visually correlated with DWIBS image (arrows). Fusion image of FDG microPET and microCT is shown in (E). Physiologic tracer uptake in heart (H) and bladder (B) in microPET image was marked (D, E).

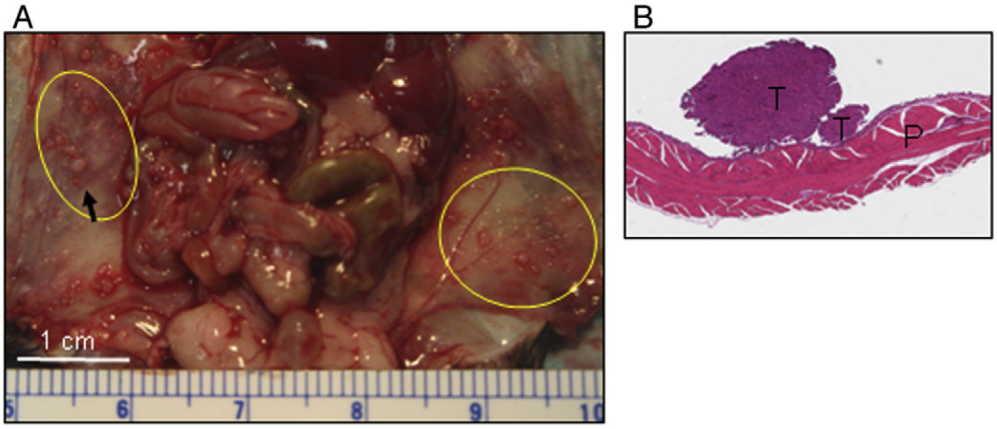

Fig. 2.

Histology of a mouse used in Fig. 1. Two circles in (A) indicate the regions including tumors that correspond to the image data (arrows) of Fig. 1, and an arrow indicates the biggest tumor. The representative tumor (T) on peritoneum (P) was stained by H&E (original magnification, ×40) (B).

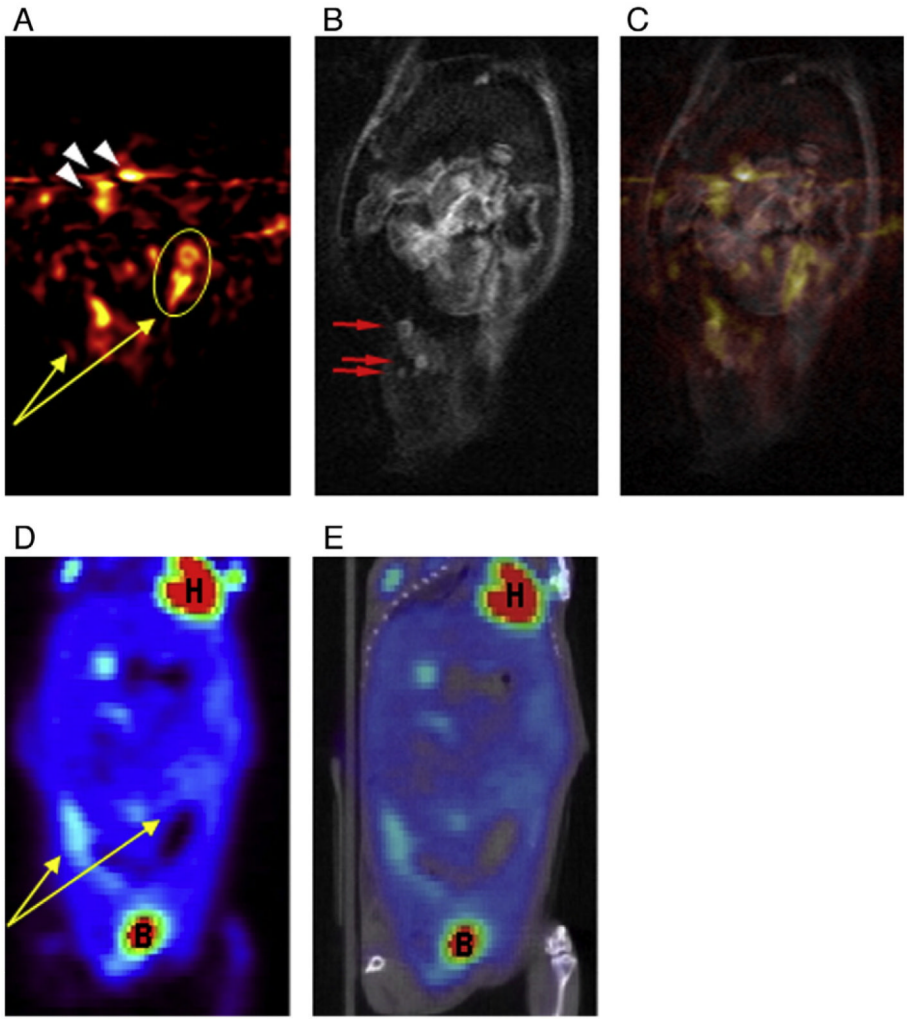

Fig. 3.

Coronal images of a mouse showing motion artifacts on DWIBS image (ventral view). DWIBS image (color coded) was obtained, highlighting several lesions (arrows and arrowheads) (A). T_2-weighted MR image showing three intermediate signal intensities (arrows) on the right abdomen (B) and a lesion was fused to a hyperintense signal of DWIBS image (C). Two hyperintense signals (arrows) on FDG microPET image (D) were correlated with DWIBS image (arrows) (A). Fusion image of FDG microPET and microCT (E). Physiologic tracer uptake in heart (H) and bladder (B) in microPET image was also marked (D, E).

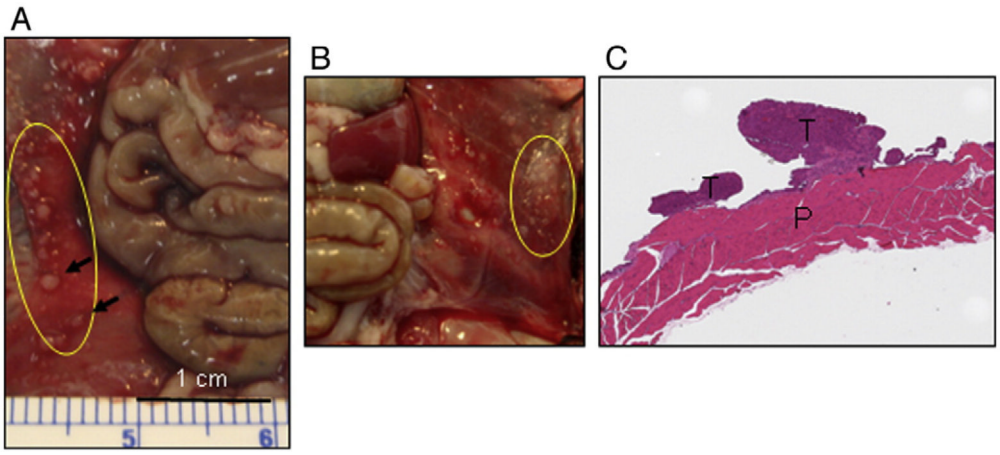

Fig. 4.

Histology of a mouse used in Fig. 3. Arrows on macroscopic appearance (A) indicate the tumors of approximately 1.02±0.02 mm^3 and 0.45±0.00 mm^3. Circles (A, B) indicate the regions containing tumors that corresponded to the image data. The representative tumor (T) on peritoneum (P) was stained by H&E (original magnification, ×40) (C).

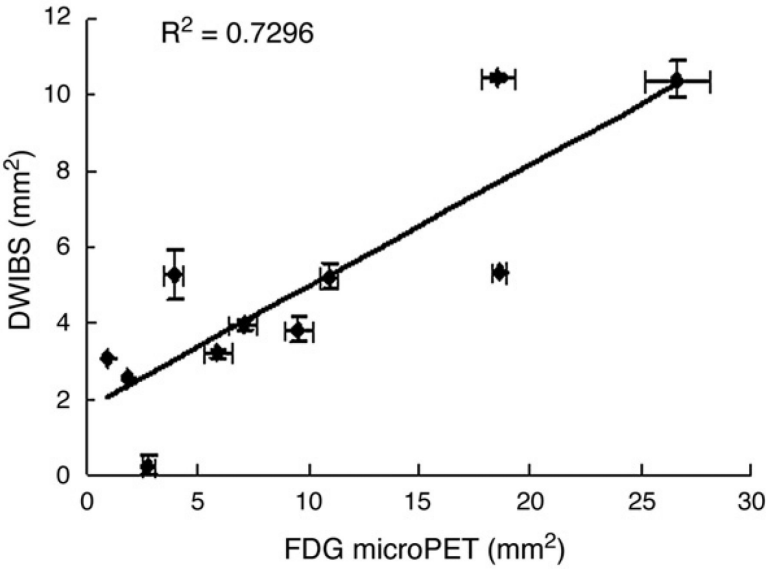

Fig. 5.

Relative area assessments of comparable lesions in both images of DWIBS and FDG microPET. The squared correlation coefficient is presented as r^2. Error bars for both modalities are indicated.